Reprinted from

MATERIALS SCIENCE & ENGINEERING A

Materials Science and Engineering A200 (1995) 55–67

Failure mechanisms during isothermal fatigue of SiC/Ti–24Al–11Nb composites

P.K. Brindley, P.A. Bartolotta

NASA Lewis Research Center, Cleveland, OH 44135, USA

ELSEVIER

MATERIALS SCIENCE AND ENGINEERING A

The journal provides an international medium for the publication of theoretical and experimental studies and reviews of the properties and behavior of a wide range of materials, related both to their structure and to their engineering application. The varied topics comprising materials science and engineering are viewed as appropriate for publication: these include, but are not limited to, the properties and structure of crystalline and non-crystalline metals and ceramics, polymers and composite materials.

Types of contributions
Original research work not already published; plenary lectures and/or individual papers given at conferences; reviews of specialized topics within the scope of the journal; engineering studies; letters to the editor.

Subscriptions
Volumes 189–204, each volume containing 2 issues, are scheduled for publication. Prices are available from the publishers upon request. Subscriptions are accepted on a prepaid basis only. Issues are sent by SAL (Surface Air Lifted) mail wherever this service is available. Airmail rates are available upon request. Please address all requests regarding orders and subscription queries to

ELSEVIER SCIENCE SA

P.O. Box 564, 1001 Lausanne, Switzerland
Telephone: (21) 3 20 73 81
Telex: 450620 ELSA CH Telefax: (21) 3 235 444

Issues are sent by surface mail after air delivery to Argentina, Australia, Brazil, Canada, China, Hong Kong, India, Israel, Japan, Malaysia, Mexico, New Zealand, Pakistan, Singapore, South Africa, South Korea, Taiwan, Thailand and the USA. Airmail rates for other countries are available on request.
For advertising rates apply to the publishers. A specimen copy will be sent on request.

US and Canadian customers may obtain information from the following.

ELSEVIER SCIENCE INC.
Attn.: Journal Information Center, 655 Avenue of the Americas New York, NY 10010, USA.
Telephone: (212) 633 3750 Telex: 420 643 AEP UI
Telefax: (212) 633 3764.

Abstracting and/or Indexing Services
American Ceramic Society; Cambridge Scientific Abstracts; Chemical Abstracts; Current Contents; Engineering Index; FIZ Karlsruhe; Fluid Abstracts; Fluidex; Glass Technology Abstracts; Inspec/Physics Abstracts; Metals Abstracts; Pascal (Centre National de la Recherche Scientifique); Physikalische Berichte; Research Alert™; Science Citation Index.

ELSEVIER

Materials Science and Engineering A200 (1995) 55–67

MATERIALS SCIENCE & ENGINEERING A

Failure mechanisms during isothermal fatigue of SiC/Ti–24Al–11Nb composites

P.K. Brindley, P.A. Bartolotta

NASA Lewis Research Center, Cleveland, OH 44135, USA

Abstract

Failure mechanisms during isothermal fatigue of unidirectional SiC/Ti–24Al–11Nb (at.%) composites have been determined by microstructural analysis of samples from tests interrupted prior to the end of life and from tests conducted to failure. Specimens from three regions of life were examined based on the maximum strain from a fatigue life diagram: Region I (high strain), Region II (mid-strain) and Region III (low strain). Crack lengths were also measured from interrupted samples and compared based on temperature (23–815 °C), region of life and numbers of cycles. Region I was controlled by fibre-dominated failure. A transition zone was observed between Regions I and II due to competition between failure mechanisms. Failure in Region II was generally described as surface-initiated cracking with varying amounts of fibre bridging. However, the specific descriptions of crack propagation through the fibres and matrix varied with strain and temperature over this broad region. Region III exhibited endurance behaviour at 23 °C with no cracking after 10^6 cycles. However at 425 °C, surface-initiated cracking was observed after 10^6 cycles with fractured fibres in the crack wake. If endurance behaviour exists for conditions of isothermal fatigue in air at temperatures of $\geqslant 425$ °C, it may only be found at very low strains and at greater than 10^6 cycles.

Keywords: Failure; Isothermal fatigue; Titanium aluminide composites

1. Introduction

Much of the research on isothermal fatigue of titanium aluminide composites has focused on the effects of mechanical or "macro" variables on material properties. For example, the $\alpha_2 + \beta$ titanium aluminide composites such as SiC/Ti–24Al–11Nb [1–9] (hereafter denoted SiC/Ti-24-11) and SiC/Ti–25Al–10Nb–1Mo [10] have been tested extensively to determine the effects of environment, temperature, strain/stress range, frequency and R-ratio on fatigue life. A limited amount of work has also been published on composites with the higher Nb content alloys (which also contain an orthorhombic phase) such as SiC/Ti–20Al–24Nb [11] (hereafter denoted SiC/Ti-20-24). Of the "macro" effects, the air environment has the most pronounced influence on isothermal fatigue life, since tests in vacuum and inert environment [12] showed an order of magnitude increase in life at 425 and 815 °C compared with tests in air (Fig. 1). Fewer studies [3,7,10] have included metallographic evidence of the microscopic events which lead to failure in SiC reinforced titanium aluminide composites during isothermal fatigue. More typically, descriptions of failure mechanisms have been determined by monitoring damage (through changes in modulus, stress and electric potential) during testing [2,3,6], through surface replication at various intervals

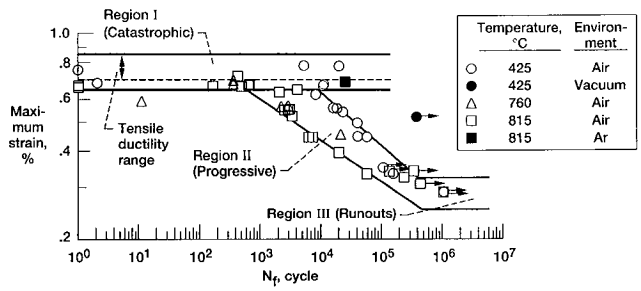

Fig. 1. Fatigue life diagram for 0° SiC/Ti-24-11 composites determined from mechanical behaviour during isothermal fatigue cycles in each region [3]. Effects of air and inert environments [12] also shown.

SSDI 0921-5093(95)07013-3

of life [6] and by examination of fracture surfaces [1–7,9–12].

Talreja [13] was the first to suggest the possible link between regions of isothermal fatigue life (as observed in a fatigue life diagram in which life was plotted on a strain basis) and distinctly different microscopic failure mechanisms. Talreja's suggestion was based on three regions of differing mechanical response of a polymer matrix composite at a single temperature, 23 °C, but metallographic information on failure mechanisms was not provided. Similarly, previous work by the present authors [3] for SiC/Ti-24-11 tested in air showed three different mechanical responses in isothermal fatigue over a range of temperatures. As described in Fig. 1, catastrophic failure was observed in the high strain region (Region I); progressive failure and large simultaneous degradations in stress and modulus were observed prior to failure in the mid-strain region (Region II); and test runouts were observed with little degradation in stress or modulus after 10^6 cycles in the low strain region (Region III). Although preliminary metallographic evidence supported the suggestion of distinct failure mechanisms in each region, metallographic examinations in each of the three regimes were incomplete. More recently, metallographic confirmation of three distinct failure mechanisms has been performed for the 23 °C isothermal fatigue of SiC/Ti-24-11 [10] and SiC/Ti–15V–3Cr–3Al–3Sn [10,14] (hereafter denoted SiC/Ti-15-3) composites and for a SiC/Ti-15-3 composite at elevated temperature in an Ar environment [14]. Some microscopic work to define failure in Region II has also been performed for isothermally fatigued SiC/Ti-24-11 composites in air at elevated temperatures [7]. In addition, fatigue crack growth of SiC/Ti-24-11 composites [15–18] has been characterized at 23 °C and the mechanism and rate of crack growth was found to be dependent on the applied stress. However, a definitive study to show differences in failure mechanisms in the three regions has not been performed for SiC/Ti-24-11 composites isothermally fatigued in air at elevated temperatures and differences within the broad, mid-strain region (Region II) have not been addressed. Furthermore, little is known about high cycle fatigue cracking of either titanium aluminide or titanium alloy composites, since few tests are performed to 10^6 cycles and post-test analysis of these samples has been limited.

Thus the purpose of the present study was to identify failure mechanisms during isothermal fatigue of a 0° SiC/Ti-24-11 composite at ambient and elevated temperatures in air. Interrupted isothermal fatigue samples and fracture surfaces of failed specimens were examined from each of the three regions of life identified in the fatigue life diagram of this composite. Relative rates of cracking were also compared based on temperature, region of life and numbers of cycles.

2. Experimental procedure

SiC/Ti–24Al–11Nb (at.%) composite plates were fabricated using the powder cloth technique [19] and matrix-only plates were made from powder alone (no binder was used). Starting materials included the SCS-6 SiC fibre manufactured by Textron, Inc., and prealloyed PREP® powder. The fibre mat was held together by a fugitive binder. The composite plates were vacuum hot pressed (VHP) using a consolidation sequence designed to remove both the powder and fibre binders. Consolidated plates were typically 15.25 cm by 5.1 cm by 0.85 mm thick and contained 3 fibre plies. Fibre volume fraction was approximately 26%. Composite specimens were wire electrodischarge machined (EDM) from the plates. The specimen design included a reduced, parallel-sided gauge section and large fillet radii of 60 mm to reduce the number of failures near the radius [3]. After EDM, the specimen surfaces were ground with 180 grit SiC paper to remove the 10 μm cladding reaction with the Mo release sheets used during the VHP operation and to remove damage due to wire EDM.

Interrupted isothermal fatigue tests were conducted using hybrid strain control at 23, 425, 760 and 815 °C. Test parameters included use of a triangular control waveform which was limited by the required maximum applied strain and zero load [3]. This method did not allow the specimen to experience compressive stresses, and by design, did not allow ratcheting to occur. A standard 12.7 mm gauge length extensometer was mounted on the edge of the sample and the strain rate used during testing was 10^{-3} s^{-1}. For the elevated temperature tests, specimens were heated in a two-zone resistance furnace [20] and the specimens were held at temperature for up to 1 h prior to testing to allow the testing equipment to stabilize. Note that 1 h at the highest test temperature of 815 °C causes negligible growth of the fibre/matrix reaction zone [21].

Microstructural analysis was performed on composite samples from interrupted tests and on samples fatigued to failure. Characterization of samples from interrupted tests consisted of surface examination for cracks by optical or scanning electron microscopy (SEM) and subsequent polishing followed by SEM and, when appropriate, wavelength dispersive X-ray spectrometry (WDS) examinations of the gauge length. Fatigue crack lengths were measured from polished sections of interrupted samples. Characterization of failed samples included SEM examination of fracture surfaces.

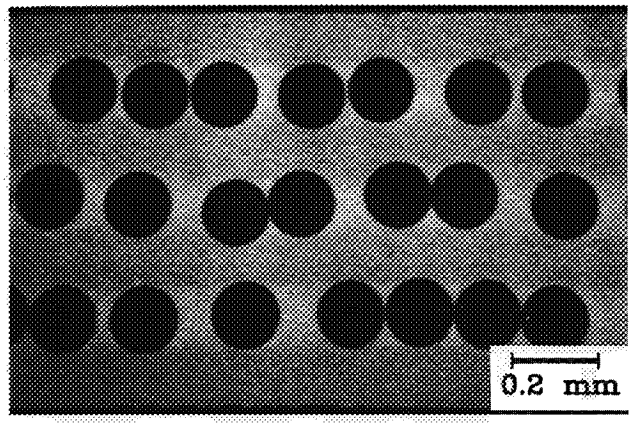

(a)

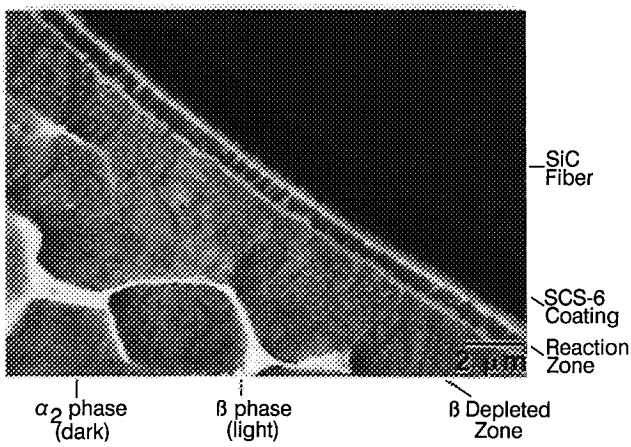

(b)

Fig. 2. Transverse cross-sections of the as-fabricated SiC/Ti-24-11 composite show (a) typical fibre distribution and (b) microstructural features of the fibre/matrix interface.

3. Results

3.1. As-fabricated microstructure

Composite cross-sections show the typical fibre distribution and features near the fibre/matrix interface in Figs. 2(a) and (b), respectively. As shown in Fig. 2(b), the matrix microstructure was comprised of equiaxed α_2 (dark phase) and β (light phase). A β-depleted zone is adjacent to the fibre/matrix reaction zone which surrounds the C-rich fibre coating. A more extensive analysis of the composite microstructure resulting from use of the powder cloth technique is given in Ref. [22].

3.2. Interrupted tests

The interrupted isothermal fatigue data for temperatures of 23, 425 and 815 °C are shown with their respective composite fatigue life plots [2,3] in Figs. 3–5. Interrupted test results were combined for the 760 and 815 °C tests in Fig. 5, since the fatigue lives at both

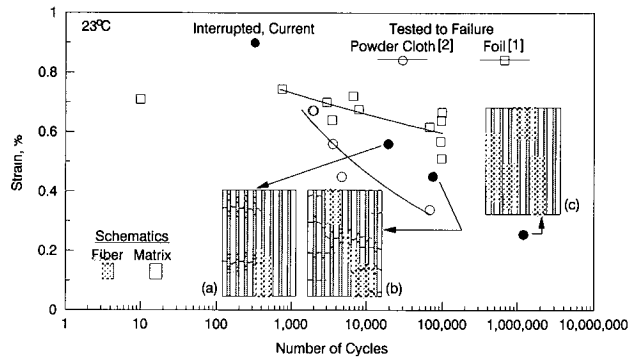

Fig. 3. Fatigue life diagram at 23 °C shows fatigue lives and conditions at which tests were interrupted in the present work. Schematics show locations of fibre and matrix cracking from interrupted tests.

these temperatures followed the same life line [2]. Schematics of longitudinal section microstructures were drawn from individual photomicrographs and show the observed locations of fibre and matrix failure in interrupted composite tests (Figs. 3–5). Example photomicrographs showing a surface-initiated fatigue crack with fibre bridging are given in Figs. 6(a) and (b) and will be discussed shortly. Interrupted test results will be presented for three regions of maximum strain: the high strain region or Region I ($\geq$ 0.65%), the mid-strain region or Region II ($\approx$0.35–0.64%) and the low strain region or Region III ($\leq \approx$0.34%). Table 1 contains the composite life data compiled from references of related work [2,3]. Table 2 contains data from interrupted tests, including numbers of cycles and numbers and lengths of cracks observed.

At 23 °C, interrupted tests were performed only in Regions II and III. Two samples were interrupted in Region II and both showed surface-initiated cracking and fibre bridging (Fig. 3, schematics (a) and (b)). Fibre cracks were observed around the matrix cracks. For both of these samples multiple cracks initiated from the sample edges. Cracking was much more extensive in the 0.45%/74 750 cycle sample; matrix cracks from both

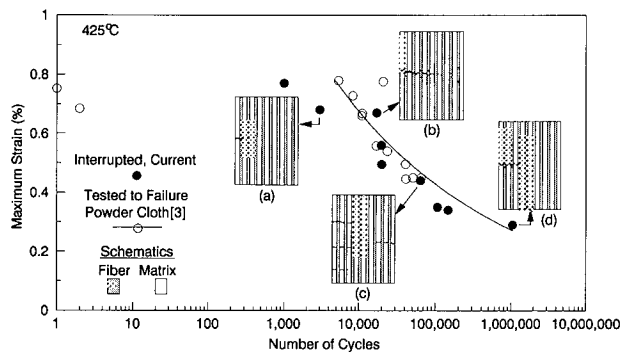

Fig. 4. Fatigue life diagram at 425 °C shows fatigue lives and conditions at which tests were interrupted in the present work. Schematics show locations of fibre and matrix cracking from interrupted tests.

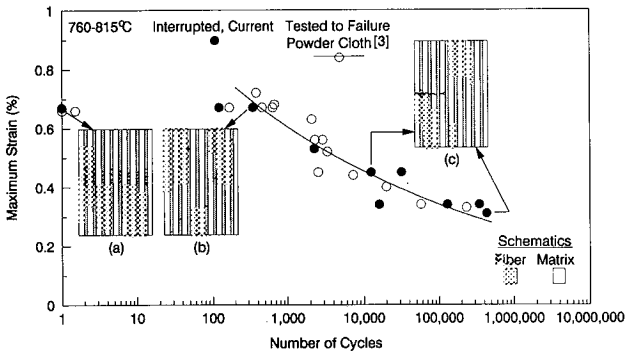

Fig. 5. Fatigue life diagram at 815 °C shows fatigue lives and conditions at which tests were interrupted in the present work. Schematics show locations of fibre and matrix cracking from interrupted tests.

edges overlapped with a central crack to cover the entire sample width. In Region III at 23 °C, no cracks were observed either on the surface or internally for the sample interrupted after 10^6 cycles at 0.27% strain (schematic (c)).

Note also from Fig. 3 that the 23 °C interrupted tests were between the 23 °C lives for SiC/Ti-24-11 composites made from powder cloth [2] and from foil [1] methods. The 23 °C samples made from powder cloth for the earlier study [2] failed in the radius and thus lives were less than the 23 °C interrupted tests of the present study (even though the same fabrication parameters, specimen design and surface preparations were used). Cracks observed in interrupted samples in the current work at 23 °C were located within the gauge section. The rough surface (from 180 grit SiC paper) of all the samples made from powder cloth may have influenced the failure location and fatigue lives at 23 °C, although it is not clear why only the earlier [2] group of specimens was affected. Specimens made from foil [1] were diamond ground and polished.

At 425 °C, surface-initiated cracking and fibre bridging were observed in all three regions of the fatigue life diagram, as shown by schematics (a)–(d) of Fig. 4. Crack initiation occurred early in the life of the composite in the high strain region, as shown by schematic (a) for the conditions of 0.68% strain/3000 cycles, which is approximately 25% of the total life. No matrix or fibre cracks had initiated after 1000 cycles at 0.77% strain, which was approximately 10% of the expected life. At approximately 100% of life in this high strain region (at 0.68% strain), the crack length was large and the fibres had failed ahead of the crack tip, as shown in schematic (b). In the mid-strain region at 425 °C, crack propagation was limited, as was fibre failure behind the crack tip even near the end of life (schematic (c)). One to four cracks were observed in polished sections (Table 2). In the low strain region at 425 °C, failure had not occurred after 10^6 cycles. However, a crack had initiated from the surface and the fibres in the crack wake were fractured, as shown in Fig. 4, schematic (d), and in Fig. 7. The crack extended through 17% of the cross-section (a crack length of 1116 μm). Long-range debonding and damage within the outer C-rich fibre coating were also visible up to 350 μm away from the fatigue crack.

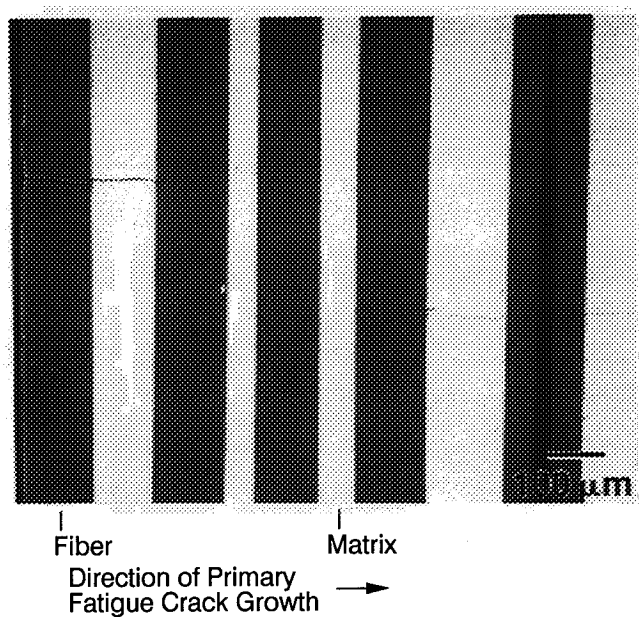

(a)

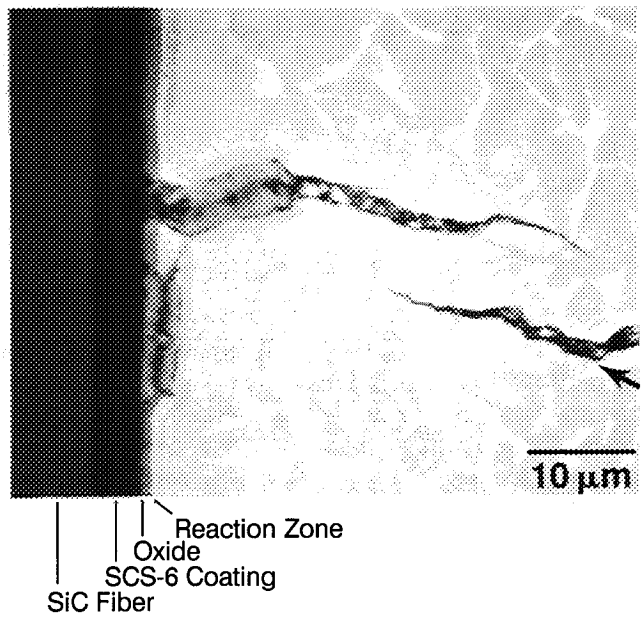

(b)

Fig. 6. Region II exhibited (a) surface-initiated cracking with fibre bridging and (b) axial cracks (shown by arrow) which initiated from interface regions near the crack tip and propagated backwards to link with the primary fatigue crack. In (b), an oxide layer is shown between the outer SCS-6 fibre coating and the reaction zone for temperatures $\geqslant$425 °C. Photos from 425 °C/0.50%/20 017 cycles sample.

Table 1
Isothermal fatigue lives of $[0]_3$ SiC/Ti–24Al–11Nb

Temperature (°C)	Maximum strain (%)	Life (cycles)
23	0.67	1 935
23	0.67	2 013
23	0.56	3 611
23	0.45	4 718
23	0.34	67 776
425	0.78	5 320
425	0.78	20 882
425	0.75	0.25
425	0.73	8 280
425	0.68	2
425	0.67	11 063
425	0.66	10 908
425	0.56	16 995
425	0.54	23 711
425	0.50	40 914
425	0.45	65 197
425	0.45	41 257
425	0.45	51 063
425[a]	0.29	1 048 743
760	0.66	0.25
760	0.56	2 904
760	0.56	2 298
815	0.72	382
815[b]	0.68	25 372
815	0.68	668
815	0.67	460
815	0.67	636
815	0.67	166
815	0.66	0.25
815	0.63	2 087
815	0.52	3 355
815	0.44	7 268
815	0.45	2 538
815	0.40	19 917
815	0.34	57 025
815	0.33	233 355

[a]Runout
[b]Inert (AR) environment

Table 2
Interrupted isothermal fatigue tests of $[0]_3$ SiC/Ti–24Al–11Nb

Temperature (°C)	Maximum strain (%)	Interrupted life (cycles)	Maximum crack length (μm)	Number of bridged cracks observed
23	0.56	19 306	3 324	5
23	0.45	74 750	4 625	9
23	0.27	1 003 500	0	0
425	0.77	1 000	0	0
425	0.68	3 000	270	1
425	0.67	17 242	2 630	1
425	0.56	19 800	822	1
425[a]	0.52	380 000	0	0
425	0.50	20 017	1 191	1
425	0.44	64 050	1 230	4
425	0.35	107 000	0	0
425	0.34	147 500	0	0
425	0.29	1 048 743	1 116	1
760	0.67	1	0	0
815	0.67	121	0	0
760	0.67	344	0	0
815	0.65	401	0	0
815	0.53	2 251	0	0
815	0.45	12 500	2 218	1
815	0.45	31 500	1 306	1
815	0.34	16 006	0	0
815	0.34	130 045	0	0
815	0.34	347 000	2 828	1
815	0.31	433 966	2 568	1

[a]Vacuum

At 815 °C, two types of fibre cracking were observed in Region I. As shown in Fig. 5, schematic (a), the high maximum strains resulted in fibre failure in a local region across the entire sample width after only 1 cycle in one sample. For another sample, interrupted after 344 cycles at the same maximum strain (0.67%), fibre cracks were random throughout the cross-section in the outer ply of fibres, as shown in schematic (b) of Fig. 5. The latter sample was polished further to expose the middle fibre row and the results were the same: fibres were cracked at random locations throughout the cross-section.

In both the mid- and low-strain regions at 815 °C, fibre bridging was evident, as shown by schematic (c) of Fig. 5. Schematic (c) also shows that the crack length for the sample in the low strain region (0.31%/434 000 cycles) was substantial and approximately the same as for the interrupted test in the mid-strain region (0.45% strain/12 500 cycles). In both samples, the crack had propagated through 40% of the sample width (a crack length of approximately 2800 μm). Only one bridging crack per sample was observed in the interrupted tests at 815 °C.

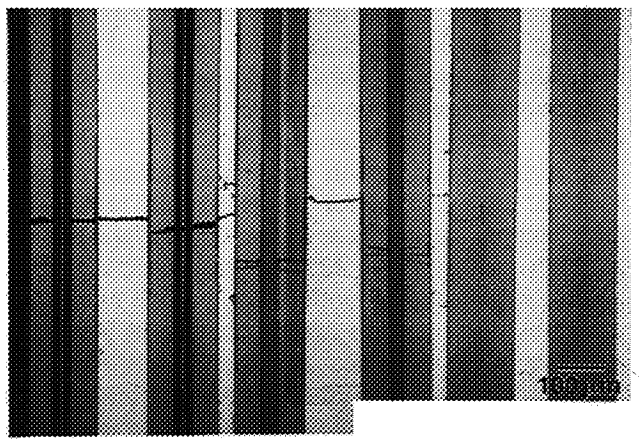

Fig. 7. A surface-initiated crack with broken fibres in the crack wake was observed for conditions of 425 °C/0.29% strain/10^6+ cycles. Surface matrix layer not shown since it crumbled during metallographic preparation.

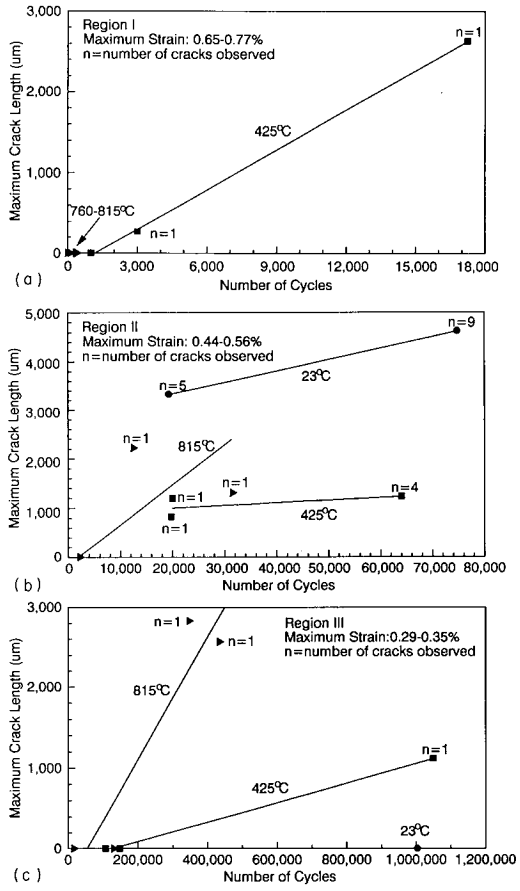

Fig. 8. Maximum crack lengths after cycling show the effects of temperature within the strain ranges of (a) Region I, (b) Region II and (c) Region III.

The effects of maximum strain and temperature on crack growth are compared in Figs. 8(a)–(c) where the length of the longest crack was plotted vs. the number of cycles for each strain region. Note that the scale for numbers of cycles changes in each figure. Since multiple cracks were observed in some samples, the numbers of cracks were also indicated beside each data point.

In Fig. 8(a) for the high strain region, it is again shown that surface-initiated cracks were not observed in interrupted tests at temperatures of 760 and 815 °C. However, once a crack initiated at 425 °C in the high strain region, crack growth was linear with the number of cycles. In Fig. 8(b) for the mid-strain region, the crack lengths and numbers of cracks were greatest for the 23 °C samples. At 425 °C, the maximum crack length remains constant with cycles, but the number of cracks observed increases from 1 after 20–30 000 cycles to 4 after $\approx 64\,000$ cycles. At 815 °C, only one main fatigue crack was observed in interrupted tests. At all temperatures crack growth was slower in the mid-strain region than in the high strain region.

In the low strain region shown in Fig. 8(c) the effect of temperature was very pronounced, since cracking occurred earlier and to a greater depth at 760–815 °C than at 425 °C. The most important points of Fig. 8(c) are that surface-initiated cracking was present after 10^6 cycles at 425 °C in the air environment, substantial crack growth occurred at elevated temperatures with these very low maximum strains and extended cycling (in excess of 100 000 cycles) was required before cracks were observed.

3.3. Microstructure of interrupted samples

As previously mentioned, an example of the surface-initiated fatigue cracks and fibre bridging described for many of the interrupted tests is shown in the backscattered SEM image of Fig. 6(a). Note that the surface matrix layer is not shown in Fig. 6(a) because it crumbled during metallographic preparation. The fragile nature of the matrix surface layer is expected to be caused by environmental embrittlement and oxidation, as will be discussed. As shown in Fig. 6(b), the SCS-6 carbon coating on the SiC fibre surface promoted fibre bridging, since the fatigue crack travelled around fibres via this coating. Also shown in Figs. 6(a) and (b) are the two directions of crack growth through the matrix: in Fig. 6(a), crack growth occurred from the free surface toward the centre of the sample. In Fig. 6(b), an axial crack is also shown which emanated from the reaction zone of the fibre ahead of the crack tip and then propagated back toward the main fatigue crack. Both directions of matrix crack growth were observed at all temperatures and regions of life where fibre bridging was observed.

Oxidation was evident within fatigue cracks at temperatures as low as 425 °C. Shown in Fig. 6(b) is a continuous layer of oxide (as determined by WDS) which formed between the outer carbon layer of the fibre and the reaction zone during fatigue testing. Areas of oxidized material were also observed near the crack tip at 815 °C after approximately 434 000 cycles (a distance of over 2500 μm from the sample surface). Furthermore, a gradient in dissolved oxygen had penetrated through the fatigue crack walls into the adjacent matrix material to a depth of 5–10 μm at 815 °C.

Oxidation of the free surfaces was also observed at 425 and 815 °C. Oxidation at 425 °C was confined to the external surfaces. However, at 815 °C, surface-connected oxidation had penetrated through the matrix to the outer fibre rows in an area away from the main fatigue crack after $\approx 434\,000$ cycles, as shown in Fig. 9(a). A narrow 1.2 mm long crack on the free surface (which was removed during polishing) was the entry point for the oxygen. It is apparent that oxygen travelled easily along the fibre interfaces once it reached the fibres, since the polished section revealed a more extensive oxidized area than was obvious from the size of the surface crack. The surface crack had been centred over the highly oxidized area shown in Fig. 9(b), in which fractured fibres were observed.

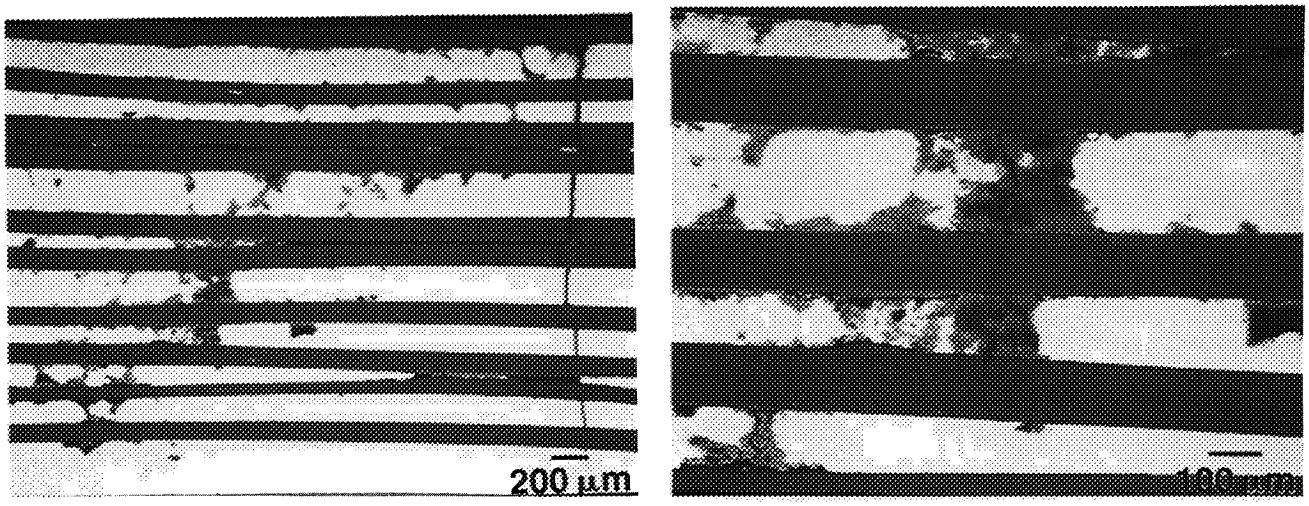

(a) (b)

Fig. 9. Primary fatigue crack and oxide penetration to the first fibre row in an area away from the main fatigue crack are shown in (a) for conditions of 815 °C/0.31% maximum strain/433 966 cycles. The highly oxidized, surface-connected region caused fibre failure as shown by the higher magnification view in (b).

3.4. Fracture surfaces

At 23 °C, the fracture surfaces of the fatigued samples were relatively featureless; the fatigued regions were not easily discerned from the overload regions. In general, the fracture surfaces looked like those of 23 °C tensile samples [23] with only short lengths of fibre pullout.

The fracture surfaces of the elevated temperature samples had distinct fatigue and overload regions. Fatigue cracks initiated along edges and at corners. Some differences in fracture surface features were observed at 425 °C. For the samples tested at higher maximum strains, the fatigue region was relatively flat, as shown in Fig. 10(a). At intermediate strains, fracture surfaces with large steps were observed, as shown in Fig. 10(b), indicating multiple fatigue cracks had propagated over considerable distances. In the fatigue region, fibres typically failed near the level of the matrix. However, the outer SCS-6 fibre coatings of fatigued fibres contained ridges, as shown in Fig. 11(a) (indicating a fretting-type damage from the fatigue cycles) which were not observed on fibre coatings in the overload regions (Fig. 11(b)). The fracture surfaces at 760 and 815 °C were generally like that of Fig. 10(a), with the exception that more fibre pullout was observed in the overload regions at the higher temperatures. At 760 and 815 °C, multiple shallow fatigue cracks were also observed on the surface below the fracture.

3.5. Fatigue life comparisons

Fig. 12 shows fatigue life comparisons at elevated temperatures for SiC/Ti-24-11 and SiC/Ti-20-24 composites made by powder cloth [3,7,11] and foil [1] methods. Note the presence of three regimes of life: Region I is shown by individual data points for lives $\leqslant 100$ cycles, Region II is shown by life lines at various temperatures and Region III is indicated by test runouts. In Region I, failure after $\leqslant 100$ cycles was observed in SiC/Ti-24-11 composites fabricated by both the powder cloth and foil methods over a range of temperatures from 23–815 °C. Comparison with SiC/Ti-20-24 in Region I was not possible, since SiC/Ti-20-24 composites were not isothermally fatigued at high maximum strains ($\geqslant 0.65\%$).

In Region II, the 23 °C fatigue life line was relatively flat at high strains and crossed over the 425 °C life line at $\approx 18\,000$ cycles. Fatigue life was degraded as temperature was increased from 150 to 815 °C. Fatigue lives at 650, 760 and 815 °C were similar for the powder cloth SiC/Ti-24-11 composites from two separate studies [3,7], for the powder cloth SiC/Ti-20-24 composite [11], and for the foil SiC/Ti-24-11 composite [1]. In Region III, test runouts were observed as previously described in this study.

4. Discussion

The results of the present study show metallographic evidence for three regimes of failure during the isothermal fatigue of SiC/Ti-24-11 composites, as summarized in Fig. 13. The discussion will be divided into sections which describe failure in Regions I–III. The identification of these regions was previously [3] based on the mechanical response of the composite and formed the basis for the present work. However, the failure mechanisms observed metallographically did not always fit neatly within these boundaries, except in general terms.

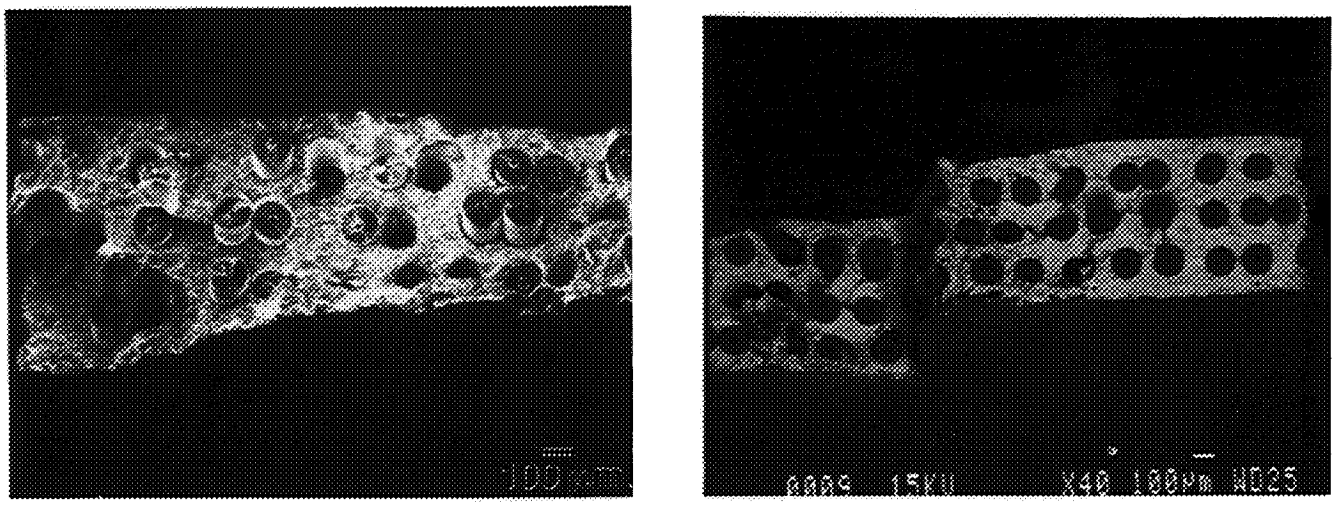

(a) (b)

Fig. 10. Fracture surfaces at 425 °C and (a) 0.73% maximum strain showed a relatively flat fatigue region and (b) 0.50% maximum strain, fracture surfaces exhibited stepped regions.

For example, all failure within Region II was surface-initiated and involved fibre bridging. However, the details of crack progression through the fibres and matrix varied over the large strain range inclusive to Region II and were further affected by temperature and the air environment. The present work also shows that transitions between regimes were complex due to competition between failure mechanisms from adjoining regions. Failure mechanisms will be compared to previous work in each of the three regimes of isothermal fatigue life.

4.1. Region I (*fibre failure*)

In the high strain region, fatigue life was unpredictable since failure occurred as early as the first 1/4 cycle or as late as that predicted from a power law curve fit of Region II. Samples tested from 23–815 °C exhibited failure in this region (Figs. 4, 5 and 12). Short lives at high strains were also common to composites of other studies with matrices of both titanium aluminide [1,3,7] and titanium alloys [14]. Furthermore, this short life behaviour was not dependent on fabrication method, since it was observed in composites fabricated by both foil [1,14] and powder [3,7] methods.

The explanation for the similarity of Region I in all these materials may be related to the common feature of the composites in this study and the studies cited above: the SCS-6 SiC fibre. Observations of cracked fibres in the absence of both matrix and surface-initiated cracks at 760 and 815 °C (Fig. 5, schematics (a) and (b)) were clear evidence that fibre failure dominated at lives $\leqslant \approx 400$ cycles. Furthermore, SCS-6 SiC fibre strengths have been shown to be degraded during fabrication of titanium aluminide composites processed by three different fabrication techniques (powder cloth [24], plasma spray [24] and foil [25,26]), resulting in bimodal Weibull distributions of extracted fibre strengths. Mean values of the extracted fibre strengths from the lower Weibull modulus region were approximately 2400 MPa [24], which corresponds to a mean failure strain of 0.6% using a fibre modulus of 400 GPa [27,28]. The 0.6% fibre failure strain corresponds approximately to the lower strain boundary for which catastrophic failure was observed in Region I. Therefore, fibre-dominated fatigue failure in the high strain region is suggested to be caused by fracture of low strength fibres which result from fabrication of these composites. This explanation accounts for both the observed temperature independence and the unpredictable fatigue lives in this high strain region. In addition, differences in distribution of low strength fibres in the as-fabricated composite may have led to the differences observed metallographically in fibre failure in Region I (local vs. cumulative fibre failure).

Other explanations have also been suggested for fibre-dominated failure during isothermal fatigue. It was suggested [14] that the debonding observed in SiC/Ti-15-3 composites at 23 °C may have led to the abrasion of the fibres' C-coatings during fatigue and subsequent fibre strength degradation, since another study [29] showed that fibre strength degradation was associated with fibres which developed damaged C-rich coatings during fatigue. However, it is not known from the present work whether the C-rich fibre coatings were damaged in Region I at 23 °C, since tests were not performed at these high levels of applied strain at this temperature. Therefore the relative contributions of low strength fibres from fabrication (as discussed above) versus low strength fibres due to abraded C-coatings during fatigue are uncertain. At elevated temperatures, creep relaxation of the matrix has also been suggested

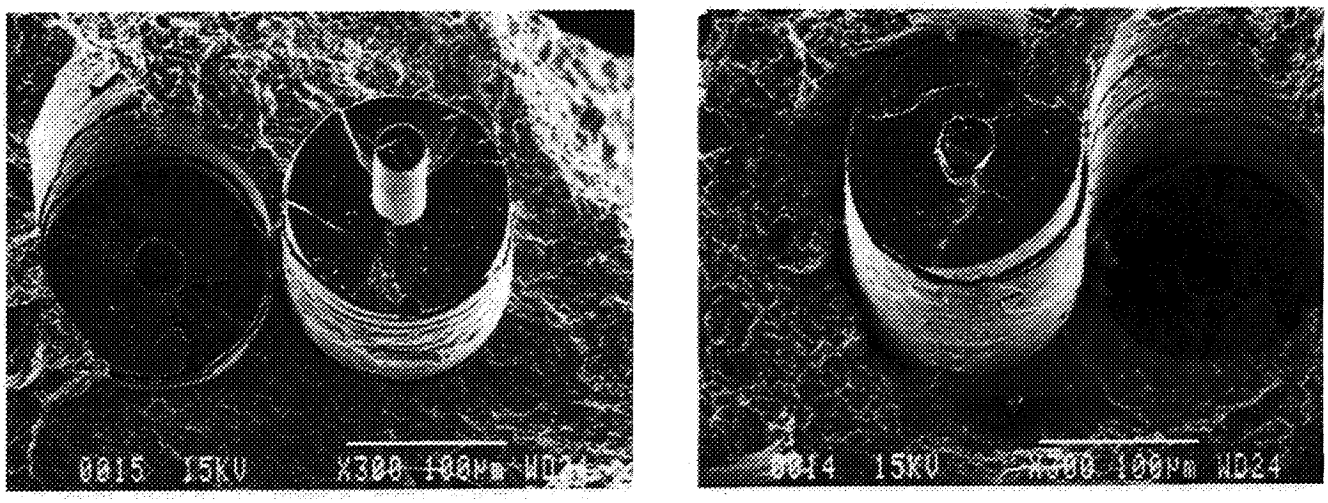

(a) (b)

Fig. 11. Fibres from elevated temperature fracture surfaces had (a) ridged C-coatings in fatigue regions and (b) relatively smooth C-coatings in tensile overload regions as shown for the 425 °C/0.50% strain/8280 cycles sample.

to result in load shedding to the fibres and subsequent fibre overload [7,14] in Region I. This mechanism is expected to contribute to failure in Region I, but it did not manifest itself in any measurable way; i.e. life was not shown to be temperature-dependent, as would be expected if stress-relaxation was the primary mechanism in this region.

4.2. Regions I and II transition

As lives approached the power law curve in the high strain regime, metallographic evidence and fracture surface evidence showed that the failure mechanism became more complex, since fibre-dominated failure competed with surface-initiated cracking, particularly at 815 °C. For example, as just discussed, one test interrupted at ≈90% of life at 815 °C showed only fibre failures (Fig. 5, schematic (b)). However, the fracture surface of another sample tested at the same maximum strain (0.67%) clearly showed surface-initiated cracking,

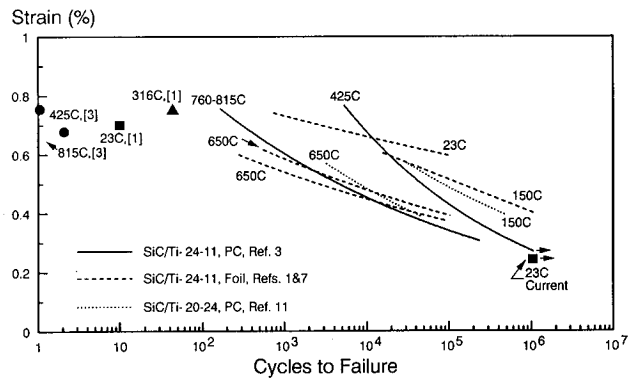

Fig. 12. The effects of temperature and fabrication method on life are shown in the fatigue life diagram for SiC/Ti–24Al–11Nb and SiC/Ti–20Al–24Nb composites.

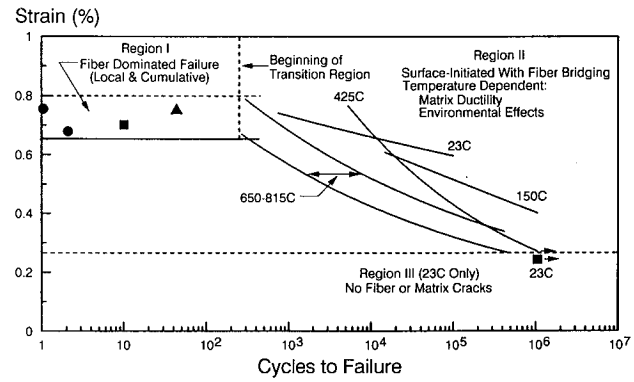

Fig. 13. Summary of isothermal fatigue failure mechanisms for SiC/Ti–24Al–11Nb composites based on metallographic evidence.

similar to that of Fig. 10(a). Thus, the high strain area at the intersection of fibre-dominated failure and surface-initiated failure can be thought of as a transition zone between the two regimes.

4.3. Region II (surface-initiated failure with fibre bridging)

Isothermal fatigue failure in the mid-strain regime was predictable; it was described by a power law fit at each temperature and was generally defined as surface-initiated cracking with varying amounts of fibre bridging. This contrasts with the Region II failure mechanism reported [14,30] for SiC/Ti-15-3 composites in which fatigue cracks were initiated internally at the fibre/matrix interface and at the Mo ribbon used to cross-weave the fibre mats.

With regard to fibre strength in Region II, abrasion of the SCS-6 fibre coating has been correlated with

strength degradation of fibres at and behind the crack tip in double-edged notched specimens of SiC/Ti-15-3 and SiC/Ti-24-11 composites [29] which were isothermally fatigued at 23 °C, as previously mentioned. It is suggested here that similar fibre strength degradation may also occur at elevated temperatures since fibres with ridged fibre coatings were observed (Fig. 11) in the fatigue areas of fracture surfaces whereas fibre coatings in the overload region were cracked but primarily smooth. Oxidation was also observed (Fig. 6(b)) between the SCS-6 coating and the reaction zone for the SiC/Ti-24-11 of the present study and for SiC/Ti-15-3 composites [30] isothermally fatigued in air at 427 °C. This oxidation at the fibre/matrix interface may also degrade fibre strength at elevated temperatures as the SCS-6 coating is removed through reaction with the air. Similarly, such oxidation would also be expected to degrade the fibre/matrix interfacial bond.

Another effect of temperature and the air environment on isothermal fatigue failure of SiC/Ti-24-11 composites can be seen in the transition from fibre-dominated failure (Region I) to surface-initiated failure (Region II) as shown in Fig. 12. At elevated temperatures, the transition to power law behaviour (Region II) occurred at lesser numbers of cycles as temperature was increased. Environmental effects on the matrix are expected to be the primary cause for the transition to surface-initiated failure at elevated temperatures, since oxidation and embrittlement rates increase as temperature increases. For example, it has been shown [31] that near surface hardening (a measure of the embrittled region) occurred after only 1 h at 800 °C in Ti-24-11 and in Ti–22Al–23Nb (denoted hereafter Ti-22-23), an orthorhombic-containing alloy similar to Ti-20-24. Surface hardening and subsequent surface cracking played a role in the fatigue failure of Ti-22-23 [11,31]. Also, as previously mentioned, 0° SiC/Ti-24-11 composites tested in vacuum [12] exhibited an order of magnitude increase in life at 425 and 815 °C compared with tests in air (Fig. 1). Similarly, the isothermal fatigue lives of SiC/Ti-15-3 composites in vacuum were increased by 4 × compared with lives in air at 427 °C [30]. Clearly, the temperature-dependent environmental effects played a major role in the transition to Region II behaviour described by power law behaviour.

Surface crack initiation at 425 °C occurred early in the life of the SiC/Ti-24-11 composite, between 10 and 25% of the expected life at a maximum strain of 0.68% (Fig. 4, schematic (a)). Thus crack propagation occupied the majority of the life of the composite in the power law region. Similarly, surface crack initiation was also observed at approximately 17% of the expected life in a SiC/Ti-24-11 composite made from foil [7] which was isothermally fatigued at 650 °C at approximately 0.48% maximum strain. These initiation times are within the range previously reported for crack initiation (between 10 and 50% of the expected life) in titanium alloy composites [14].

The details of surface-initiated failure in Region II were further affected by temperature, since differences in fibre and matrix cracking were observed metallographically (as shown by the schematics in Figs. 3–5). For example, more surface cracks were observed at 23 °C than at elevated temperatures and cracks propagated faster at 23 °C than at elevated temperatures (Fig. 8(b)). This is presumably due to the low matrix ductility at room temperature. The numbers of cracks at 23 °C also increased with increasing number of cycles. At 23 °C, fibre cracks were observed above and below the matrix cracks, but not directly in line with the matrix crack (Fig. 3, schematics (a) and (b)). However, the 23 °C fracture surfaces from Region II showed fibre and matrix failure at approximately the same level. Therefore the cracked fibres apparently continued to carry load and fractured again at final sample failure to obtain a fracture surface with little fibre pullout. Similar fibre fracture behaviour was reported for the 150 °C isothermal fatigue of another SiC/Ti-24-11 composite in the mid-strain region [7].

Despite the enhanced surface-initiated cracking at 23 °C, the fatigue life line at 23 °C was relatively flat compared with the life lines at elevated temperatures (Fig. 12). This is probably due to the combination of more effective fibre bridging at 23 °C and little/no environmental effects at 23 °C.

At 425 °C, matrix ductility increased [23], but the effects of increased matrix ductility on surface cracking were countered at this temperature by the effects of the air environment [12,31]. That is, increased matrix ductility should act to decrease the number of surface cracks, but embrittlement at longer times should favour multiple crack formation. The apparent result is that multiple crack initiation at 425 °C was not observed in interrupted tests until after 64 000 cycles, as shown in Fig. 4, schematic (c) (i.e. at lower maximum strains and longer time at temperature). Fibres failed in the crack wakes and sample failure occurred upon overload. An interrupted test from the high strain end of Region II (Fig. 4, schematic (b)) showed a different progression of cracking. One primary fatigue crack was observed and fibres failed close behind the crack tip (presumably due to the higher maximum strain). Fibres ahead of the crack tip failed just prior to matrix overload at the end of life. The fracture surfaces were generally consistent with the observed differences in crack propagation as a function of strain and time to failure in Region II. Fracture surfaces from the higher strain samples at 425 °C showed one main fatigue crack (Fig. 10(a)) and at lower strains (i.e. longer times at temperature), stepped areas of connected fatigue cracks were observed (Fig. 10(b)).

At 760–815 °C and at strains in both the intermediate and lower portions of Region II, propagation of a single

crack was generally observed and fibres failed in the crack wake (Fig. 5, schematic (c)). Since severe oxidation of the fibre/matrix interface (between the C-coating and the reaction zone) and oxygen penetration deep within the fatigue crack were observed at these temperatures, environmental effects again dominated fatigue failure and apparently caused propagation to be concentrated in one primary crack. Surface embrittlement was also more severe at these temperatures; multiple, shallow fatigue cracks were evident on the free surfaces below the primary fatigue crack at 760–815 °C. These shallow cracks indicate an embrittled area and they contribute to the overall decrease in load-bearing area. Furthermore, at very long times, penetration of oxygen through a crack in the free surface (away from the main fatigue crack) to the first fibre row can also occur, causing local fibre failure (Figs. 9(a) and (b)). These examples metallographically illustrate the consequences of operating for extended times at temperatures beyond the oxidative capability of the matrix.

4.4. Region III (mechanical endurance behaviour: 10^6 cycles)

As previously mentioned, prior work [3] indicated that endurance behaviour may be approached in this SiC/Ti-24-11 composite since little degradation in stress or modulus was observed after 10^6 cycles. It was metallographically shown (Fig. 3, schematic (c)) that an endurance limit may exist at 23 °C since no fibre or matrix cracks were observed after 10^6 cycles at 0.27% maximum strain. However, further testing is required to determine the threshold strain for endurance behaviour. From Fig. 12, if the 23 °C life line was extrapolated along the same curve to 10^6 cycles, endurance behaviour would be expected to occur at substantially higher maximum strains than 0.27%.

In fatigue crack growth studies of SiC/titanium aluminide and titanium alloy composites [15–18], crack arrest at low stresses was associated with fibre bridging by unbroken fibres near the crack tip. In contrast, after 10^6 cycles at 425 °C (Fig. 4, schematic (d)), surface-initiated cracking with fibre bridging had extended to a depth of 1116 μm. There is strong evidence to suggest that crack arrest may not be expected in the 10^6 cycle regime at 425 °C, including the broken fibres observed in the crack wake and the long-range debonding (up to 350 μm) at the fibre/matrix interface, both of which negate the effects of fibre bridging. Furthermore, there is some evidence to suggest that severe oxidation around fibres leads to a damaged fibre/matrix interface and to fibre fracture at very low maximum strains (0.31%) as shown in Figs. 9(a) and (b). This does not necessarily mean that endurance behaviour will not be found for this composite at elevated temperatures. However, it does imply that the fatigue crack observed after 10^6 cycles at 425 °C may continue to grow with cycling as long as the maximum strain is greater than the fracture strain of both the expected embrittled matrix region at the crack tip and of the environmentally exposed fibres in the crack wake. Keeping in mind that the crack length data (Fig. 8(c)) indicates $> 100\,000$ cycles is required to initiate cracks at low maximum strains, the present work points to the need for long-term cycling at very low strains and elevated temperatures followed by metallographic examination to more fully characterize fatigue crack growth of SiC/titanium aluminide composites in air.

4.5. Fatigue life comparisons

Fig. 12 clearly shows that the fatigue lives of SiC/titanium aluminide composites fabricated by powder cloth [19] and foil methods were similar in Regions I and II. Thus, both the powder cloth [19] and foil methods are viable fabrication routes which resulted in equivalent properties.

Comparison of the titanium aluminide composites with an $\alpha_2 + \beta$ matrix microstructure with those with an $\alpha_2 + \beta +$ orthorhombic matrix microstructure also reveals many similarities. As shown in Fig. 12, the isothermal fatigue life lines of SiC/Ti-20-24 and SiC/Ti-24-11 composites were the same at two temperatures, 150 and 650 °C. These composites also utilized the same fibre and have matrices which hardened similarly at elevated temperatures in the air environment [31]. The orthorhombic-containing matrix also exhibited surface-initiated cracking [11,31] in isothermal fatigue tests of the standalone matrix. Thus, the higher Nb-content titanium aluminide composites which contain an additional orthorhombic phase in their matrix microstructure, such as SiC/Ti-20-24 and SiC/Ti-22-23, may also exhibit the same isothermal fatigue failure mechanisms as the SiC/Ti-24-11 composites of the present study.

5. Summary and conclusions

1. The three regions of fatigue life observed for SiC/Ti–24Al–11Nb composites in a fatigue life diagram provided a general guideline for the determination of microscopic failure mechanisms. However, distinctly different failure mechanisms did not neatly fit within the boundaries of the fatigue life diagram due to environmental effects at elevated temperatures and the competition of failure mechanisms in overlapping regions.
2. Local and random (cumulative) fibre failure were observed metallographically at high maximum

strains ($\geq 0.65\%$) for lives ranging from 1/4 to ≈ 400 cycles and at temperatures from 23–815 °C. The lower strain boundary of Region I corresponded approximately to the failure strain of low strength fibres present in SiC/titanium aluminide and SiC/titanium alloy composites fabricated by several techniques. Thus, isothermal fatigue failure in Region I was dominated by fibre failure and appears to be strongly influenced by the statistical distribution of low strength fibres. However, the difficulty in predicting failure in this region makes design applications impractical at these high maximum applied strains.

3. The transition between Regions I and II is complex as mechanisms in these regions compete, especially at temperatures where environmental effects are most severe (i.e. 760–815 °C) as shown by the intersection of the power law curve with the fibre-dominated region.
4. Failure in Region II was shown to be surface-initiated with varying amounts of fibre bridging. Lives were described by power law behaviour and were dependent on temperature. At 23 °C, more effective fibre bridging and little influence of the air environment resulted in a fatigue life line which was relatively flat at high maximum strains despite extensive cracking. At elevated temperatures, the air environment degraded the matrix and the fibre/matrix interface (through oxidation and embrittlement) and led to fibre failure at very long times. Thus, life was degraded as temperature was increased.
5. Endurance limit behaviour was not always associated with test runouts after 10^6 cycles. Endurance behaviour was attained at 23 °C with no cracking after 10^6 cycles. However, the threshold strain for endurance behaviour at 23 °C remains undefined. At 425 °C, surface-initiated cracking with fibre fracture in the crack wake was observed after 10^6 cycles. Due to environmental effects and ineffective fibre bridging, it is suggested that this crack will continue to grow beyond 10^6 cycles as long as the maximum applied strain exceeds the failure strain of both the embrittled matrix at the crack tip and the environmentally exposed fibre. Thus, endurance behaviour at elevated temperatures may only be expected at very low strains ($< 0.29\%$).
6. Since Ti–24Al–11Nb and Ti–20Al–24Nb type matrices exhibited similar environmentally induced surface hardening behaviour and surface-initiated fatigue cracks and since composites with these matrices exhibited similar isothermal fatigue lives in air, SiC/Ti–20Al–24Nb type composites may also exhibit fatigue failure mechanisms similar to SiC/Ti–24Al–11Nb composites.

Acknowledgement

Dr D.A. Woodford is gratefully acknowledged for helpful discussions regarding endurance behaviour.

References

[1] M.L. Gambone, *Rep. WRDC-TR-89-4145*, Vol. II, 1990 (Wright Laboratories).
[2] P.K. Brindley, P.A. Bartolotta and R.A. MacKay, in *HITEMP Review 1989: Advanced High Temperature Engine Materials Engine Technology Program*, NASA CP-10039, NASA Lewis, Cleveland OH, 1989, p. 52-1.
[3] P.A. Bartolotta and P.K. Brindley, in G.C. Grimes (ed.), *ASTM STP-1120*, Vol. 10, Philadelphia PA, 1992, p. 192.
[4] J.M. Larsen, K.A. Williams, S.J. Balsone and M.A. Stucke, in S.H. Whang, C.T. Liu, D.P. Pope, J.O. Stiegler (eds.), *High Temperature Aluminides and Intermetallics*, TMS/ASM International, 1990, p. 521.
[5] S.M. Russ and T. Nicholas, in P.R. Smith, S.J. Balsone and T. Nicholas (eds.), *Titanium Aluminide Composites*, WL-TR-91-4020, Wright-Patterson AFB, Dayton OH, 1991, p. 431.
[6] B.R. Kortyna and N.E. Ashbaugh, in P.R. Smith, S.J. Balsone and T. Nicholas (eds.), *Titanium Aluminide Composites*, WL-TR-91-4020, Wright-Patterson AFB, Dayton OH, 1991, p. 467.
[7] T.P. Gabb and J. Gayda, in P.R. Smith and W.C. Revelos (eds.), *Titanium Matrix Composites*, WL-TR-4035, Wright-Patterson AFB, Dayton OH, 1992, p. 292.
[8] T. Nicholas and S.M. Russ, *Mater. Sci. Eng., A153* (1992) 514.
[9] T.P. Gabb and J. Gayda, in *Life Prediction Methodology for Titanium Matrix Composites*, ASTM, Philadelphia PA, 1995, in press.
[10] S.M. Jeng, P. Alassoeur and J.-M. Yang, *Mater. Sci. Eng., A148* (1991) 67.
[11] T.P. Gabb and J. Gayda, in *HITEMP Review 1993: Advanced High Temperature Engine Materials Technology Program*, NASA CP-19117, NASA Lewis, Cleveland OH, 1993, p. 33-1.
[12] P.K. Brindley and P.A. Bartolotta, in *HITEMP Review 1991: Advanced High Temperature Engine Materials Technology Program*, NASA CP-10082, NASA Lewis, Cleveland OH, 1991, p. 46-1.
[13] R. Talreja, in *Fatigue of Composite Materials*, Technomic Publishing, Lancaster PA, 1987.
[14] B.S. Majumdar and B.L. Lerch, in P.R. Smith and W.C. Revelos (eds.), *Titanium Metal Matrix Composites II*, WL-TR-93-4105, Wright-Patterson AFB, Dayton OH, 1993, p. 409.
[15] P. Kantzos, J. Eldridge, D.A. Koss and L.J. Ghosn, *Mater. Res. Soc. Symp. Proc.*, Vol. 273, MRS, Pittsburgh PA, 1992, p. 135.
[16] D.L. Davidson, in P.R. Smith and W.C. Revelos (eds.), *Titanium Matrix Composites*, WL-TR-4035, Wright-Patterson AFB, Dayton OH, 1992, p. 306.
[17] R. John, S.G. Kaldon and N.E. Ashbaugh, in P.R. Smith and W.C. Revelos (eds.), *Titanium Metal Matrix Composites II*, WL-TR-93-4105, Wright-Patterson AFB, Dayton OH, 1993, p. 270.
[18] S.M. Jeng, P. Alassoeur and J.-M. Yang, *Mater. Sci. Eng., A154* (1992) 11.
[19] J.W. Pickens, R.D. Noebe, G.K. Watson, P.K. Brindley and S.L. Draper, *Rep. NASA TM-102060*, 1989 (NASA Lewis Research Center).
[20] P.K. Brindley, *US Patent No. 5,015,825*, 1991.
[21] P.K. Brindley, P.A. Bartolotta and S.J. Klima, *Rep. NASA TM-100956* , 1988 (NASA Lewis Research Center).
[22] S.F. Baumann, P.K. Brindley and S.D. Smith, *Metall. Trans. A, 21* (1990) 1559.

[23] P.K. Brindley, S.L. Draper, J.I. Eldridge, M.V. Nathal and S.M. Arnold, *Metall. Trans. A, 23* (1992) 2527.
[24] R.A. MacKay, S.L. Draper, A.M. Ritter and P.A. Seimers, *Metall. Trans. A, 25* (1994) 1443.
[25] P.R. Smith, J.A. Graves, C.G. Rhodes, M.R. James and J.R. Porter, in P.R. Smith and W.C. Revelos (eds.), *Titanium Matrix Composites* , WL-TR-4035, Wright-Patterson AFB, Dayton OH, 1992, p. 115.
[26] J. Porter, in P.R. Smith and W.C. Revelos (eds.), *Titanium Metal Matrix Composites II*, WL-TR-93-4105, Wright-Patterson AFB, Dayton OH, 1993, p. 382.
[27] J.A. DiCarlo, in R.A. Bradley, D.E. Clark, D.C. Larsen and J.O. Steigler (eds.), *Whisker- and Fiber-Toughened Ceramics*, ASM International, Metals Park OH, 1988, p. 1.
[28] J. Jackson and D.R. Spriggs, in *Air Force Contract F33657-86-C-2136, Interim Report No. 2*, 1987 (Wright Laboratories).
[29] P. Kantzos, J. Eldridge, D.A. Koss and L.J. Ghosn, *Mater. Res. Soc. Symp. Proc.*, Vol. 273, MRS, Pittsburgh PA, 1992, p. 135.
[30] B.A. Lerch, in *HITEMP Review 1990: Advanced High Temperature Engine Materials Technology Program*, NASA CP-10051, NASA Lewis, Cleveland OH, 1990, p. 35-1.
[31] W.J. Brindley and J.L. Smialek, in *HITEMP Review 1993: Advanced High Temperature Engine Materials Technology Program*, NASA CP-19117, NASA Lewis, Cleveland OH, 1993, p. 34-1.

Instructions for Authors

SUBMISSION OF PAPERS

Manuscripts for the main part of the journal should be submitted to the Editor-in-Chief, Professor H. Herman, or for authors in Japan to Professor M. Koiwa:

Professor Herbert Herman
Department of Materials Science and Engineering
State University of New York at Stony Brook
Long Island, NY 11794-2275, USA
Fax: +1 (516) 632 8052

Professor Masahiro Koiwa
Department of Metal Science and Technology
Faculty of Engineering
Kyoto University
Yoshida-Honmachi, Sakyo-ku
Kyoto 606-01, Japan
Fax: +81 (75) 751 7844

Manuscripts for the Letters Section should be submitted as follows:

For authors in Europe

Professor G. Kostorz
ETH Zurich
Institut für Angewandte Physik
CH-8093 Zurich, Switzerland
Fax: +41 (1633) 1105

For authors in Japan

Professor Masahiro Koiwa
Japan

For authors in North and South America and the rest of the world

Professor Herbert Herman
USA

Manuscripts

Three copies should be submitted to the Editor, in double-spaced typing on pages of A4 size and with wide margins (Letters should not exceed 2000 words and a maximum of 5 figures). All tables and illustrations should bear a title or legend.

An *abstract* should accompany reviews, original papers and Letters. It should present (preferably in 100–150 words; 50 words or less for Letters) a brief and factual account of the contents and conclusions of the paper, and an indication of the relevance of new material.

References should be indicated by numerals in square brackets, introduced consecutively and appropriately in the text.

References must be listed on separate sheet(s) at the end of the paper. Every reference appearing in the text should be quoted in the reference list, and *vice versa*. When reference is made to a publication written by more than two authors it is preferable to give only the first author's name in the text followed by "*et al.*". However, in the list of references the names and initials of all authors must be given.

Three sets of figures should be submitted. One set of line drawings should be in a form suitable for reproduction, drawn in Indian ink on drawing or tracing paper (letter height, 3–5 mm). Alternatively, such illustrations may be supplied as high contrast, black-and-white glossy prints. Duplicate original micrographs should be provided wherever possible to facilitate the refereeing process. Magnifications should be indicated by a ruled scale bar on the micrograph. Captions to illustrations should be typed in sequence on a separate page.

All abbreviated terms must be defined when first used (both in the abstract and in the text) and authors must express all quantities in SI units, with other units in parentheses if desired.

Authors in Japan please note that information about how to have the English of your paper checked, corrected and improved (before submission) is available from: Elsevier Science (Japan), 20-12 Yushima 3-chome, Bunkyo-ku, Tokyo 113; Tel: (03) 3833-3821; Fax: (03) 3836-3064.

Further information

All questions arising after the acceptance of manuscripts, especially those relating to proofs, should be directed to: Elsevier Editorial Services, Mayfield House, 256 Banbury Road, Oxford OX2 7DH, UK (tel. +44 1865 314900; fax. +44 1865 314990).

0921-5093/95/$9.50

Printed in The Netherlands